Open Access Research Journal of
Engineering and Technology
Journals home page: https://oarjpublication/journals/oarjet/
ISSN: 2783-0128 (Online)

OARJ OPEN ACCESS RESEARCH JOURNALS

(RESEARCH ARTICLE)

STRESS FIELD ANALYSIS FOR CIRCULAR TUNNELS IN JOINTED GRANITE ROCK MASS: A PARAMETRIC FINITE ELEMENT STUDY

Mani Shrestha *

Department of Geotechnical Engineering, College of Civil Engineering, Tongji University, Shanghai 200092, China.
* Corresponding Author

ORCID Details
Mani Shrestha: https://orcid.org/0009-0000-9135-9489

Open Access Research Journal of Engineering and Technology, 2026, 11(02), 035–042

Publication history: Received on 30 September 2026; revised on 09 November 2026; accepted on 11 November 2026

Article DOI: https://doi.org/10.53022/oarjet.2026.11.2.0074

Copyright © 2026 Author(s) retain the copyright of this article. This article is published under the terms of the Creative Commons Attribution License 4.0

ABSTRACT

This study examines stress redistribution around a 10 m diameter circular tunnel, with its crown at 50 m depth, in jointed granite. A two-dimensional plane-strain finite element model was built in Phase2 (RS2), with linear elastic intact rock and a set of fully persistent joints governed by a Coulomb slip criterion. Three stages were analyzed: the initial in-situ stress, unsupported excavation and excavation with an idealized stiff lining. Joint dip (θ = 15°, 30° and 45°) and joint spacing (S = 5, 11 and 22 m) were varied one at a time about a reference case (θ = 45°, S = 11 m). Unsupported excavation raised the major principal stress (σ_1) at the crown from 1.07 to 2.23 MPa, within 1.2–4.4% of the Kirsch solution, while the minor principal stress (σ_3) fell to near zero. The joints superimposed localized perturbations where they met the tunnel wall: a mesh-dependent σ_1 peak of about 9.6 MPa and a small tensile σ_3 of about −0.29 MPa. Because these stresses are far below the strength of intact granite, joint slip and block loosening, rather than failure of the intact rock, govern stability. Closer joint spacing increased the number, and lower joint dip the intensity, of these concentrations. A lining activated without prior ground relaxation kept stresses within about 3% of in-situ values, which represents an idealized upper bound on support effectiveness.

Keywords: Tunnel stability; Jointed rock mass; Stress redistribution; Finite element analysis; Kirsch solution; Parametric study

1 INTRODUCTION

Tunnelling through jointed rock masses is one of the most demanding problems in underground geotechnical engineering. Geological discontinuities such as joints, bedding planes and faults govern the stress distribution, the deformation pattern and the potential failure modes around an excavation. The interaction between the in-situ stress and a discrete joint network produces highly localized stress concentrations, which may lead to block loosening, tensile cracking and progressive collapse if the opening is not adequately supported [1, 2].

Granite has a high intact strength but fails in a brittle manner and often contains regular joint sets that greatly reduce the effective strength of the rock mass. Under excavation-induced unloading, pre-existing joints can slip or open and form preferential failure planes, which are difficult to capture with equivalent-continuum models alone [3].

Representing the joints explicitly within a finite element framework provides a more realistic description of this behavior.

Hoek and Brown [1] laid the foundations for the stress analysis of underground excavations, and the Kirsch solution remains the reference for the stresses around circular openings [2, 4]. Barton et al. [5] showed from tunnel case records that the number of joint sets, the joint spacing and the joint surface condition control stability and support demand. Using the distinct element method, Shen and Barton [6] showed that joint spacing governs the size and shape of the disturbed zone around tunnels, and laboratory and physical model tests have shown that joint dip, spacing and density control the failure of jointed granite [7, 8].

Finite element programs with joint elements are widely used in design practice. For preliminary design, a simple parametric study that is checked against a closed-form solution can show where joint-controlled stress concentrations arise around the opening and how far the excavation disturbance extends into the rock mass. Such a study also makes clear which results depend on the joints and which follow from classical elasticity.

This paper presents a finite element study, carried out in Phase2 [9], of a circular tunnel in granite crossed by a persistent joint set. Its objectives are: (i) to quantify the redistribution of the principal stresses caused by excavation and to verify it against the Kirsch solution; (ii) to examine the influence of joint dip (θ = 15°, 30° and 45°) and joint spacing (S = 5, 11 and 22 m) on the stress field; and (iii) to assess a stiff lining as an idealized limiting case of support.

2 MATERIALS AND METHODS

2.1 Numerical model, geometry and boundary conditions

A plane-strain finite element model was built in Phase2 (RS2, Rocscience) [9] (Fig. 1). The model domain is 70 m wide and 90 m high. The tunnel has a diameter D = 10 m, its crown at 50 m depth and its center at 55 m depth, and the lateral and bottom boundaries lie 3D (30 m) from the tunnel wall. Displacements are fixed on the base and the lateral sides, and the top surface is free. The in-situ stress is generated by gravity with a unit weight γ = 22 kN/m^3 and a lateral stress coefficient K_0 = 1.0. This isotropic ratio was chosen so that any asymmetry in the results can be attributed to the joints. Because horizontal stresses at shallow depth often exceed the vertical stress [10], the use of K_0 = 1.0 is a limitation of the study (Section 3.7).

Stresses were sampled along two measurement lines: Line 1, vertical, from the ground surface to the tunnel crown; and Line 2, horizontal, at 30 m depth, that is 2D above the crown. Table 1 summarizes the model parameters.

Table 1: Summary of model parameters

Parameter	Value	Description
Tunnel diameter (D)	10 m	Circular cross-section
Depth to crown (h)	50 m	Overburden depth
Model domain	70 m (W) × 90 m (H)	Boundaries 3D from the tunnel wall
Rock type	Granite	Linear elastic intact rock
Unit weight (γ)	22 kN/m^3	Granite unit weight
Lateral stress coefficient (K_0)	1.0	Isotropic in-situ stress
Joint dip (θ)	15°, 30°, 45°	Reference: 45°
Joint spacing (S)	5 m, 11 m, 22 m	Reference: 11 m
Boundary conditions	Fixed sides and base; free top	Plane strain

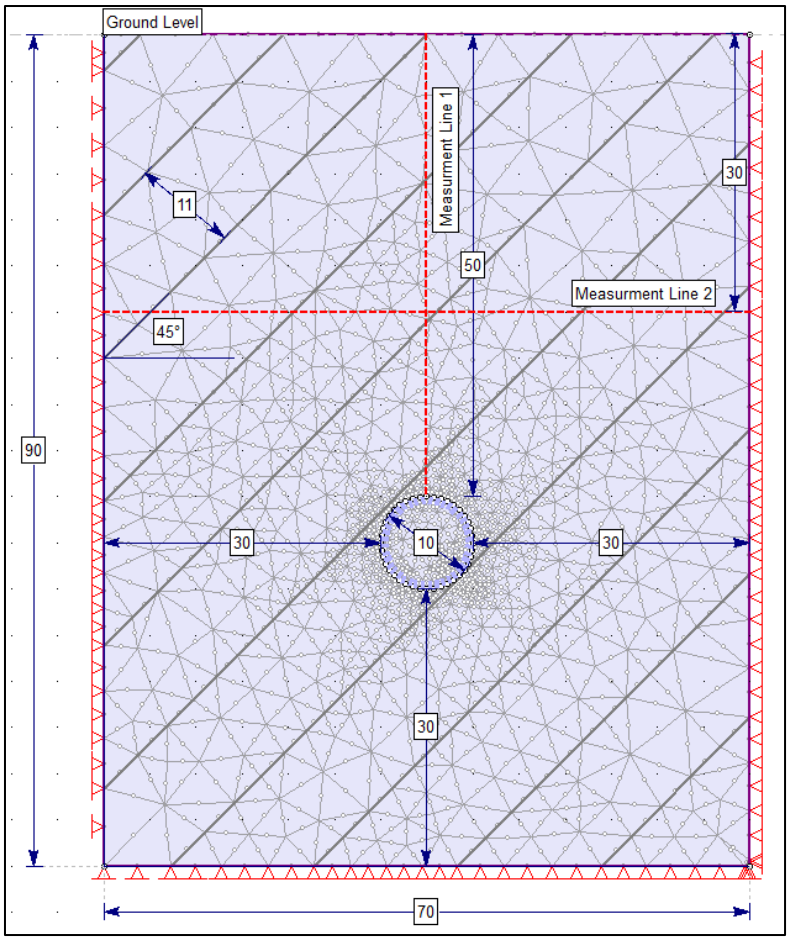


Figure 1: Model geometry (dimensions in m), finite element mesh, joint network (θ = 45°, S = 11 m) and measurement lines

2.2 Material properties

The intact granite is linear elastic with Young's modulus E = 50 GPa and Poisson's ratio ν = 0.25, which are typical of granite [11]. Intact rock properties are used, rather than rock mass properties, because the joints are modelled explicitly. The elastic assumption for the intact rock is justified by the low stress level. The crown σ_1 (about 2.2 MPa) and the local peak (about 9.6 MPa) are only 1–2% and 4–10%, respectively, of the uniaxial compressive strength of granite (100–250 MPa). Both are well below the ratio of about 0.4 at which brittle damage initiates around underground openings [12]. Non-linear behavior is therefore concentrated on the joints.

The joints follow a Coulomb slip criterion with friction angle φ = 30°, cohesion c = 0, normal stiffness k_n = 10 GPa/m and shear stiffness k_s = 1 GPa/m. These values represent smooth, weathered granite joints: φ = 30° lies within the range of residual friction angles of such joints [13], zero cohesion is conservative, and the stiffnesses fall within published ranges [14]. The concrete lining is modelled with liner elements with E = 30 GPa and thickness t = 0.3 m.

2.3 Joint representation and discretization

The joint set consists of parallel, fully persistent planes that cross the whole model. A graded triangular mesh conforms to the joint traces, along which joint elements resolve slip and opening, and the mesh is refined around the excavation (Fig. 1). In the reference case, two joints intersect or closely approach the tunnel boundary. No formal mesh-sensitivity study was performed. Instead, the near-field stresses are verified against the Kirsch solution (Section 3.3), and the local peaks at joint–boundary intersections, which are mesh-dependent, are interpreted qualitatively.

2.4 Analysis stages and parametric cases

Three analysis stages were considered (Fig. 2): Stage 1, the initial in-situ stress; Stage 2a, unsupported excavation; and Stage 2b, excavation with a stiff lining. The lining is activated in the same stage as the excavation, so no ground relaxation precedes support. This "wished-in-place" assumption defines a limiting case, not a realistic installation sequence (Section 3.4). Results are presented in detail for the reference case (θ = 45°, S = 11 m). The joint geometry was varied

one parameter at a time about this reference, with θ = 15°, 30° and 45° at S = 11 m and S = 5, 11 and 22 m at θ = 45°. This gives five joint configurations, each analyzed through the three stages.

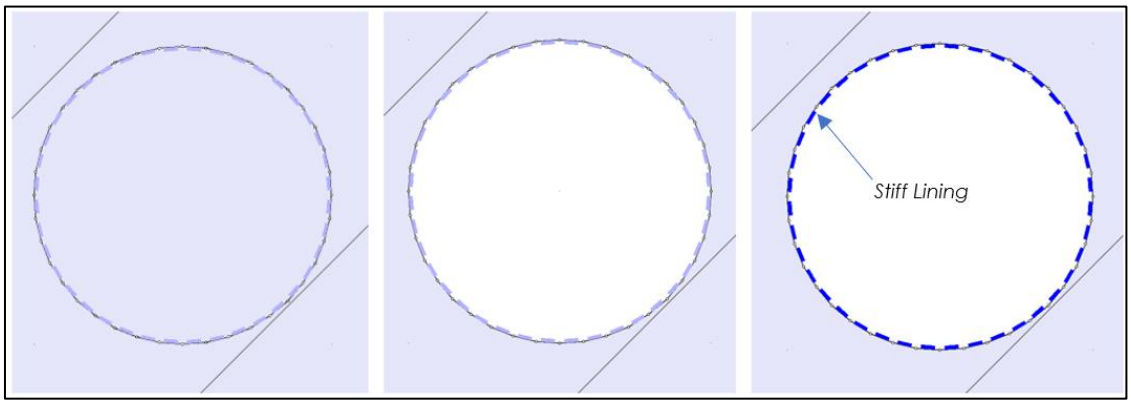


Figure 2: Analysis stages, from left to right: (a) initial in-situ stress; (b) unsupported excavation; (c) excavation with stiff lining

2.5 Analytical verification

For a circular opening of radius a in an elastic medium under an isotropic far-field stress p, the Kirsch solution [2, 4] gives the tangential stress σ_θ and radial stress σ_r at a radial distance r from the center of the opening as

$$\sigma_\theta = p(1 + a^2/r^2), \quad \sigma_r = p(1 - a^2/r^2) \qquad (1)$$

At the tunnel boundary (r = a), Eq. (1) gives $\sigma_\theta = 2p$ and $\sigma_r = 0$. Eq. (1) assumes a homogeneous, isotropic, linear elastic medium without discontinuities. It therefore provides a check on the continuum part of the numerical response, but it has no counterpart for the local effects of the joints.

3 RESULTS AND DISCUSSION

3.1 Initial in-situ stress state

In the initial state (Fig. 3), σ_1 and σ_3 increase with depth under gravity. At the future crown (50 m depth), σ_1 = 1,065.7 kPa and σ_3 = 980.5 kPa, close to the overburden stress γz = 1,100 kPa. The difference between them and the minor lateral variation of σ_1 reflect limited slip on the cohesionless joints under gravity loading. The concentrations near the base of the model, where the joints meet the fixed boundary, are boundary artefacts.

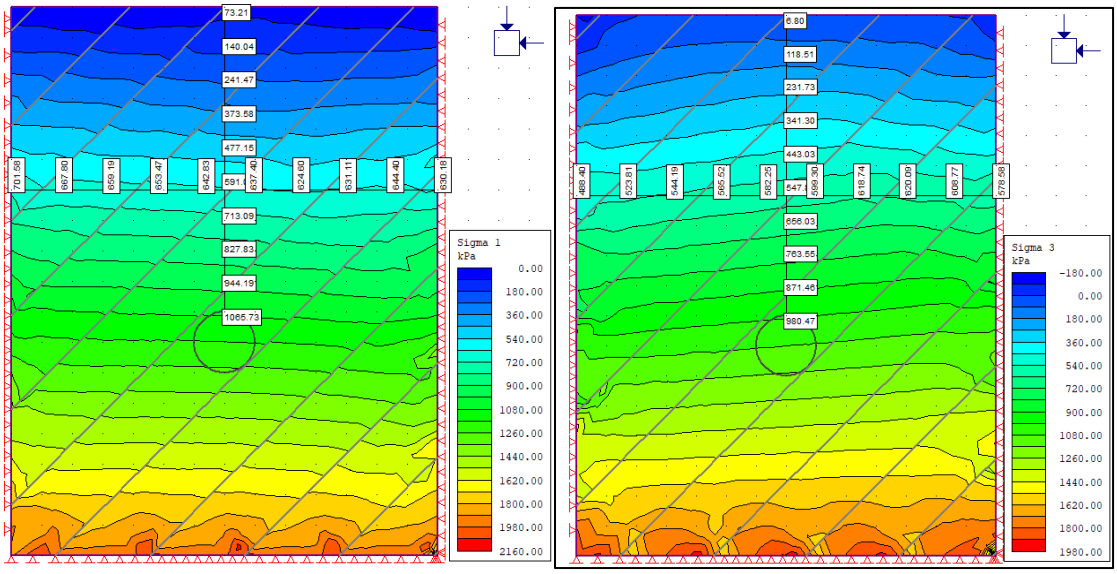


Figure 3: Contours of (a) σ_1 and (b) σ_3 (kPa) for Stage 1, the initial in-situ stress

3.2 Unsupported excavation

Unsupported excavation (Fig. 4) raises σ_1 at the crown from 1,065.7 to 2,225.9 kPa, a factor of 2.09, which is the classical tangential stress concentration at a circular opening (Section 3.3). The joints superimpose a local perturbation. In the lower-right quadrant, where a joint meets the wall at an acute angle, σ_1 reaches about 9,600 kPa within the thin rock wedge between the joint and the boundary. Because the elastic stress at such a sharp corner is theoretically unbounded, this value is mesh-dependent; it indicates the location, rather than the precise magnitude, of the joint-controlled concentration.

At the crown, σ_3 drops from 980.5 to 8.4 kPa, as expected, since the radial stress vanishes at a free boundary. A small tensile σ_3 of about −285 kPa develops next to the joint on the lower wall. This is far below the tensile strength of intact granite, which is of the order of 10 MPa [11]. However, the cohesionless joints have no tensile strength, so the tension indicates joint opening and slip, which can loosen the wedges bounded by the joints and the excavation [2, 6]. Joint-controlled block loosening, rather than failure of the intact rock, is therefore the governing instability mechanism.

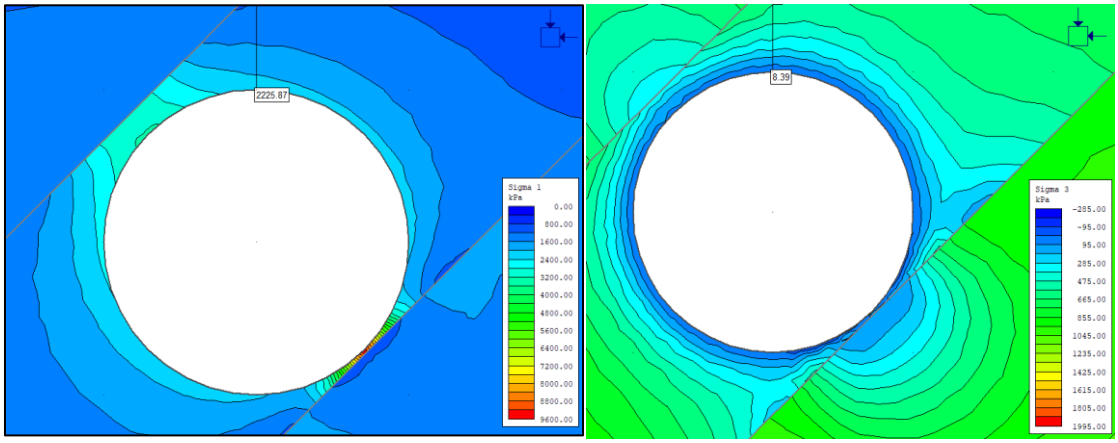


Figure 4: Contours of (a) σ_1 and (b) σ_3 (kPa) around the unsupported excavation (Stage 2a, reference case)

3.3 Verification against the Kirsch solution

Because the far-field stress p varies over the height of the tunnel, three estimates were used: the computed in-situ σ_1 at the crown (1,065.7 kPa), and the overburden stress at crown level (1,100 kPa) and at the tunnel center (1,210 kPa). Eq. (1) then gives a boundary tangential stress of 2,131, 2,200 and 2,420 kPa, respectively, against the computed 2,225.9 kPa, which corresponds to differences of +4.4%, +1.2% and −8.0%. The computed radial stress at the crown (8.4 kPa) is consistent with zero. Eq. (1) also predicts that the excess of σ_θ over p falls to 25% and 11% of its boundary value at 0.5D and 1D above the crown, which agrees with the extent of disturbance found along the measurement lines (Section 3.6). The local peaks at joint intersections, by contrast, have no continuum counterpart [6].

3.4 Supported excavation with a stiff lining

With the stiff lining, the σ_1 and σ_3 contours are practically identical to those of the initial state (Fig. 3) and are therefore not shown. The crown σ_1 is 1,094.0 kPa, compared with 1,065.7 kPa in situ, and the profiles along the measurement lines are compared in Figs. 5 and 6. This result follows from activating the lining together with the excavation, so that no ground relaxation precedes support. In practice, much of the displacement occurs ahead of the face before the support is installed, so the lining carries only part of the load and the rock undergoes greater stress redistribution. The supported case is therefore an idealized upper bound on lining effectiveness, not the expected field performance. A realistic assessment requires simulating the relaxation before support, for example with the convergence–confinement method, and checking the lining capacity.

3.5 Effect of joint orientation and spacing

Table 2 summarizes the parametric cases for unsupported excavation. Numerical values are given for the reference case. For the other cases, trends were identified by comparing their contour plots with those of the reference case, and they are reported qualitatively.

Table 2: Parametric results for unsupported excavation

θ (°)	S (m)	Maximum σ_1 (kPa)	Minimum σ_3 (kPa)	Assessed risk
45	11 (reference)	≈ 9,600	−285 (tensile)	Moderate to high (zone next to the joint)
30	11	Higher than reference	More negative than reference	High (steeper stress gradients)
15	11	Highest	Most negative	Highest (oblique joint–wall intersections)
45	5	Multiple peaks	Multiple tensile zones	Amplified (more joint intersections)
45	22	Fewer peaks	Fewer tensile zones	Reduced (fewer joint intersections)

Note: values for the non-reference case608s are qualitative, from comparison of contour plots with the reference case.

3.5.1 Effect of joint orientation

Reducing θ from 45° to 15° at S = 11 m increased the stress concentrations at joint–boundary intersections. For a circular opening with $K_0 = 1$, θ does not change the number of joints crossing the tunnel, but it controls where and at what angle the joints meet the perimeter. Because σ_1 is tangential and $\sigma_3 \approx 0$ at the boundary, a cohesionless joint slips where the angle between its normal and the tangential direction exceeds φ [11]. A plausible explanation is that flatter joints produce such oblique intersections near the crown and invert, forming thin wedges that are exposed both to the full tangential stress and to gravity. This interpretation is consistent with discontinuum and laboratory results [6, 7].

3.5.2 Effect of joint spacing

At θ = 45°, on average about D/S joints cross the opening, that is about two for S = 5 m and at most one for S = 22 m. Each intersection creates its own concentration, so the closest spacing produced multiple σ_1 peaks and more tensile σ_3 zones, whereas S = 22 m produced fewer. For S ≥ D, the response also depends on the position of the joint relative to the tunnel, which was not varied. The trend agrees with the control of the disturbed zone by joint spacing reported by Shen and Barton [6] and with the joint-density threshold observed in physical models of granite tunnels [8].

3.6 Vertical and horizontal stress profiles

Along Line 1 (Fig. 5), the unsupported case departs from the in-situ profile mainly within about 1D of the crown for σ_1 and 0.5D for σ_3, consistent with Eq. (1). As the sampling interval is about 0.56D, these extents are approximate. Along Line 2 (Fig. 6), σ_1 changes by less than about 3%, but σ_3 is reduced by about 10–14% over much of the line. This reduction is well above the value of about 4% predicted by Eq. (1) at this distance ($r \geq 5a$). It is attributed to slip on the persistent joints, which transmit stress relief into the far field. A boundary clearance of 3D may therefore not fully remove boundary effects on the far-field stresses, although the verified near-field results are unaffected. In the lined case, stresses deviate from the in-situ values by less than about 3% along both lines.

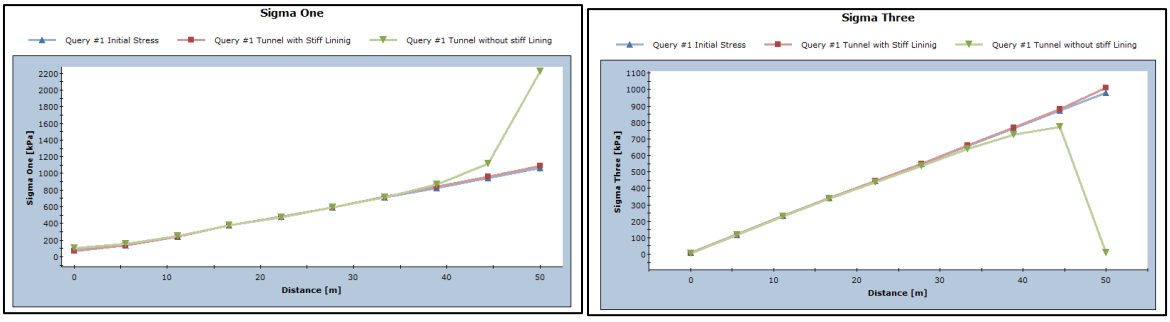


Figure 5: Distribution of (a) σ_1 and (b) σ_3 along Line 1 (vertical, from the ground surface to the crown) for the three stages

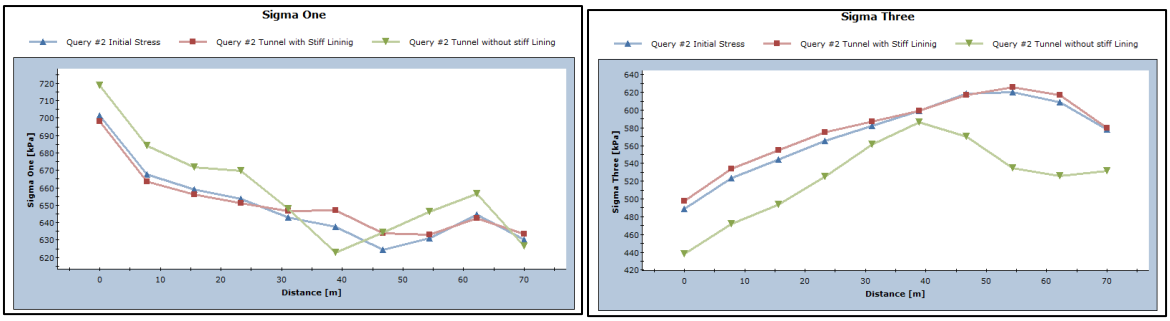


Figure 6: Distribution of (a) σ_1 and (b) σ_3 along Line 2 (horizontal, at 30 m depth) for the three stages

3.7 Limitations

The results should be read with the following limitations in mind. First, the in-situ stress is isotropic (K_0 = 1.0), whereas horizontal stresses at shallow depth commonly exceed the vertical stress; an anisotropic stress field would change both the Kirsch concentration and the location of joint slip. Second, the joints are fully persistent and the joint position relative to the tunnel was not varied, so the effect of non-persistent joints and of joint position, which matters when S ≥ D, is not captured. Third, no mesh-sensitivity study was performed, and the local peaks at joint–boundary intersections are interpreted only qualitatively. Fourth, the parametric trends for the non-reference cases are qualitative. Fifth, the lining is wished in place and its capacity is not checked. Finally, the intact rock is elastic, the analysis is two-dimensional, and the results have not been compared with field measurements.

4 CONCLUSION

A plane-strain finite element model with explicitly modelled joints was used to examine how excavation redistributes stresses around a shallow circular tunnel in jointed granite. The main conclusions are as follows.

- The continuum part of the response follows classical elasticity. Excavation roughly doubled the tangential stress at the crown (factor 2.09), in close agreement with the Kirsch solution, and removed the radial stress at the boundary. The disturbance of σ_1 extended about one tunnel diameter above the crown and that of σ_3 about half a diameter.
- The joints add localized effects with no continuum counterpart: a high but mesh-dependent compressive peak in the thin wedge where a joint meets the wall, a small tensile zone next to the joint, and a 10–14% relief of σ_3 transmitted along the persistent joints to two diameters above the crown.
- Joint geometry controls these effects. Closer spacing increased the number of joint–boundary concentrations, and a lower dip increased their intensity.
- A lining installed with no prior relaxation kept the stresses close to their in-situ values; this is an upper bound on support effectiveness, not a prediction of field behavior.

Because the induced stresses are far below the strength of intact granite, stability at this depth is governed by joint slip, joint opening and block loosening. Support design should therefore address joint-bounded wedges, particularly where joints cut the boundary obliquely or are closely spaced. Future work should report quantitative results for a full factorial set of joint geometries and positions, assess mesh sensitivity, simulate relaxation before support and check lining capacity, and consider anisotropic in-situ stress, elasto-plastic behavior, non-persistent joints and validation against field data.

STATEMENTS ON COMPLIANCE WITH ETHICAL STANDARDS

Acknowledgments

The authors thank the Department of Geotechnical Engineering, College of Civil Engineering, Tongji University, for technical and institutional support.

Disclosure of conflict of interest

The authors declare no conflicts of interest regarding this manuscript.

REFERENCES

[1] Hoek E, Brown ET. Underground excavations in rock. London: Institution of Mining and Metallurgy; 1980.

[2] Brady BHG, Brown ET. Rock mechanics for underground mining. 3rd ed. Dordrecht: Springer; 2004.

[3] Jing L. A review of techniques, advances and outstanding issues in numerical modelling for rock mechanics and rock engineering. Int J Rock Mech Min Sci. 2003;40(3):283-353.

[4] Kirsch G. Die Theorie der Elastizität und die Bedürfnisse der Festigkeitslehre. Z Ver Dtsch Ing. 1898;42:797-807.

[5] Barton N, Lien R, Lunde J. Engineering classification of rock masses for the design of tunnel support. Rock Mech. 1974;6(4):189-236.

[6] Shen B, Barton N. The disturbed zone around tunnels in jointed rock masses. Int J Rock Mech Min Sci. 1997;34(1):117-25.

[7] Yang XX, Jing HW, Tang CA, Yang SQ. Effect of parallel joint interaction on mechanical behavior of jointed rock mass models. Int J Rock Mech Min Sci. 2017;92:40-53.

[8] Xu HS, Li SJ, Xu DP, Jang Q, Liu L, Zheng MZ, et al. Investigation of parallel joint density thresholds for granite tunnel failure based on physical model experiments and multiscale monitoring techniques. Sci Rep. 2025 Aug 6;15(1):28729.

[9] Rocscience Inc. RS2 (Phase2): 2D finite element analysis for rock and soil [Internet]. Toronto: Rocscience Inc.; 2024 [cited 2026 Nov 7]. Available from: https://www.rocscience.com/software/rs2

[10] Brown ET, Hoek E. Trends in relationships between measured in-situ stresses and depth. Int J Rock Mech Min Sci Geomech Abstr. 1978;15(4):211-5.

[11] Goodman RE. Introduction to rock mechanics. 2nd ed. New York: Wiley; 1989.

[12] Martin CD, Kaiser PK, McCreath DR. Hoek–Brown parameters for predicting the depth of brittle failure around tunnels. Can Geotech J. 1999;36(1):136-51.

[13] Barton N, Choubey V. The shear strength of rock joints in theory and practice. Rock Mech. 1977;10(1-2):1-54.

[14] Bandis SC, Lumsden AC, Barton NR. Fundamentals of rock joint deformation. Int J Rock Mech Min Sci Geomech Abstr. 1983;20(6):249-68.